Ferroquadrupolar lattice instability in an antiferromagnetically ordered state in single-crystalline DyCuGe

Isao Ishii,[1,*] Kanna Sunazaki,[1] Koji Araki,[2] Makoto Shoji,[1] Kentaro Isobe,[1] Alexander V. Andreev,[3] and Takashi Suzuki[1,†]

[1]*Department of Quantum Matter, AdSE, Hiroshima University, Higashi-Hiroshima 739-8530, Japan*
[2]*Department of Applied Physics, National Defense Academy, Yokosuka, Kanagawa 239-8686, Japan*
[3]*FZU Institute of Physics, Czech Academy of Sciences, Na Slovance 2, 182 21 Prague, Czech Republic*

(Received 13 March 2024; accepted 19 April 2024; published 1 May 2024)

We report on the specific heat, magnetic properties, and ultrasonic measurements of a single-crystalline DyCuGe. We reveal an antiferromagnetic ordering in the (001) plane at $T_N = 7.4$ K, which is higher than the reported transition temperature of polycrystalline samples. The transverse elastic moduli show a pronounced softening down to T_N due to interlevel quadrupole-mediated interactions between the ground and excited Kramers doublets. Below T_N, we further detected a huge softening accompanied by ultrasound attenuation in the transverse C_{44} mode, suggesting a lattice instability. Our experimental and calculated results manifest that ferroquadrupolar interactions give rise to the lattice instability even in an antiferromagnetically ordered state.

DOI: 10.1103/PhysRevB.109.195102

I. INTRODUCTION

Rare-earth-based compounds with localized f electrons show intriguing physical phenomena due to the spin and orbital degrees of freedom, such as multipolar ordering and superconductivity [1–3]. Recently, group-theoretical classification of multipolar ordering including an odd-parity multipole has also been established [4–6]. Under a crystal electric field (CEF), compounds with higher symmetry, such as a cubic structure, possessing an orbitally degenerate ground state of the CEF have been mainly studied. By contrast, compounds with lower symmetry, such as an orthorhombic structure, have a singlet or Kramers doublet ground state with no quadrupole degeneracy. However, an interlevel multipole-mediated interaction between the ground state and excited states activates even in low-symmetry compounds. This situation often originates from a small energy splitting of the CEF states, like a quasidegenerate state.

We have reported existence of quadrupole-mediated interactions in heavy-rare-earth compounds having the Kramers doublet ground state [7–14]. $4f$ electronic states in these compounds are under the trigonal or orthorhombic CEF, and an energy splitting between the ground and excited doublets is relatively small. It is noteworthy that $DyNi_3Ga_9$ shows a ferroquadrupolar ordering accompanied by a chiral-helical magnetic ordering [7,15], $Dy_3Ru_4Al_{12}$ shows a magnetic-field-induced reentrant multipolar ordering [10], and ErNiAl shows a ferroquadrupolar ordering in a magnetically ordered state [13].

In the present study, we paid attention to the Dy-based compound DyCuGe, which has the hexagonal LiGaGe-type structure (space group: $P6_3mc$) [16,17]. Physical properties were reported only in polycrystalline samples [18–20]. The electrical resistivity exhibits a metallic behavior [20]. An antiferromagnetic (AFM) ordering at 6.0 or 5.2 K, of which the ordered structure is AFM along the b axis or canted AFM, respectively, was reported [18–20]. No magnetic moment of Cu and Ge ions was supposed [17].

The effective magnetic moment of the polycrystalline DyCuGe estimated from the magnetic susceptibility is 10.7 μ_B or 10.8 μ_B, which corresponds to the theoretical value of the free Dy^{3+}, 10.6 μ_B [18,20]. Because DyCuGe has the CEF effect, the Dy^{3+} 16-fold multiplet (total angular momentum $J = 15/2$) splits into eight Kramers doublets under the hexagonal CEF. If an energy splitting between the ground and excited doublets is relatively small, multipole-mediated interactions are expected to activate also in this compound.

Ultrasonic measurements are a powerful tool to investigate quadrupole-mediated interactions, because a strain induced by ultrasound bilinearly couples to a corresponding quadrupole moment [21–29]. In the present study, we succeeded to synthesize a single-crystalline DyCuGe sample. To elucidate the phase transition and multipole-mediated interactions in DyCuGe, we conducted the specific heat, magnetic properties, and ultrasonic measurements on a single-crystalline sample. In consequence, we observe a lattice instability in an AFM ordered state and discuss its origin by considering quadrupole-mediated interactions within the CEF approach.

II. EXPERIMENTAL DETAILS

A single crystal of DyCuGe was grown by the modified Czochralski method in a tri-arc furnace on a copper water-cooled bottom under an argon protective atmosphere. Tungsten rod was used as a seed, pulling speed was 15 mm/h. The single-crystalline state of the pulled cylinder was confirmed by the backscattering Laue method. The high structural and compositions quality of the crystal was confirmed by powder x-ray diffraction. The lattice parameters of the hexagonal crystal structure are $a = 4.238$ Å and $c = 7.251$ Å.

*ish@hiroshima-u.ac.jp
†tsuzuki@hiroshima-u.ac.jp

TABLE I. v (m/s) at 2 K for each measured mode and calculated Debye temperature θ_D (K) in DyCuGe.

C_{11}	C_{33}	C_{44}	C_{66}	θ_D
3667	3297	2429	2644	244

A commercial physical property measurement system (PPMS) was used for the specific heat measurement with a ^{3}He cryostat from 0.4–300 K. Magnetic susceptibility and magnetization were measured from 2–300 K and up to 9 T, respectively, using PPMS with a vibrating sample magnetometer. The magnetic field was applied using a superconducting magnet in all measurements.

The temperature dependence of the elastic moduli C_{11}, C_{33}, C_{44}, and C_{66} was measured between 1.8 and 150 K using a phase-comparison pulse-echo method and orthogonal phase-detection technique [30,31]. Ultrasound attenuation was measured simultaneously. The moduli, C_{11} and C_{33}, are related to the longitudinal acoustic modes with $\boldsymbol{k} \parallel \boldsymbol{u} \parallel [100]$ and $\boldsymbol{k} \parallel \boldsymbol{u} \parallel [001]$, respectively, where $\boldsymbol{k}$ and $\boldsymbol{u}$ are the propagation and displacement directions of the ultrasound, respectively. The transverse elastic moduli, C_{44} and C_{66}, were measured by ($\boldsymbol{k} \parallel [001]$, $\boldsymbol{u} \parallel [100]$) and ($\boldsymbol{k} \parallel [100]$, $\boldsymbol{u} \parallel [120]$) configurations, respectively. The elastic modulus, C, is related to the sound velocity, v, by $C = \rho v^2$, where $\rho = 8.793\ \mathrm{g/cm^3}$ is the room-temperature mass density. The absolute value of v was determined at 2 K for each mode using the sample lengths and the time interval between pulse echoes (Table I).We calculated the Debye temperature, θ_D, using an average v value for longitudinal and transverse waves [32]. We used $LiNbO_3$ transducers with a fundamental resonance frequency of about 30 and 20 MHz for the longitudinal and transverse modes, respectively.

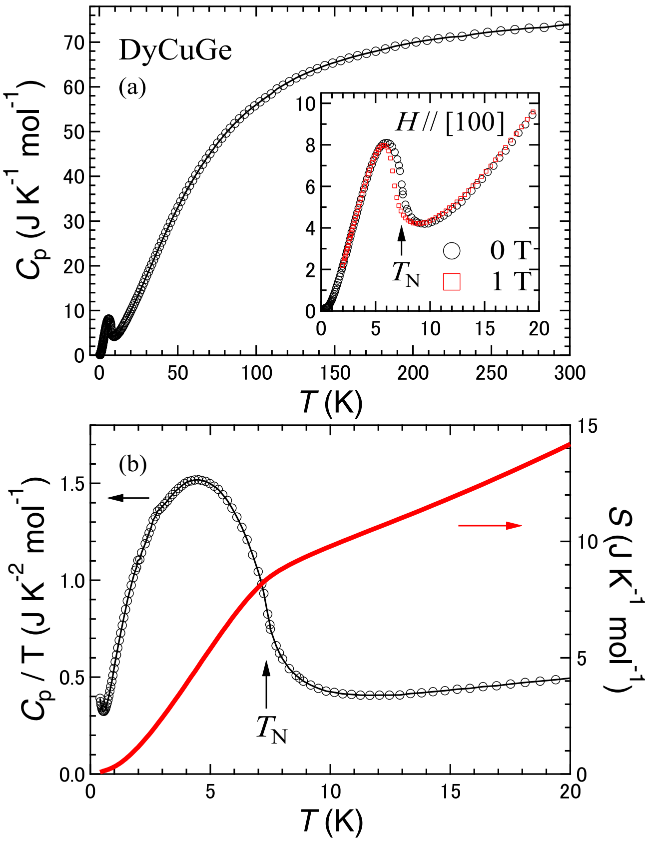

FIG. 1. (a) Temperature dependence of the specific heat C_p at zero field in DyCuGe. The inset represents the same data on an expanded temperature scale below 20 K. We also measured C_p in a magnetic field of 1 T applied along [100]. (b) Temperature dependence of the specific heat divided by the temperature C_p/T (left axis) and entropy S (right axis).

III. RESULTS AND DISCUSSION

A. Specific heat and magnetic properties

Figure 1(a) shows the temperature dependence of the specific heat, C_p, at zero magnetic field. C_p exhibits a distinct peak around 7 K, indicating a phase transition. We defined the phase transition temperature as $T_N = 7.4$ K, which is the temperature of the largest slope of C_p [the inset of Fig. 1(a)] and a peak of the magnetic susceptibility [Fig. 2(a)]. T_N of the single-crystalline DyCuGe increases up to 7.4 K compared with reported values of polycrystalline samples [18–20]. T_N decreases by applying a magnetic field of 1 T along [100]. Below T_N, other obvious peak is not detected down to 0.4 K within our experimental resolution. At high temperatures, C_p reaches 74.0 J/(K mol) at 300 K, which is almost the value of the Dulong-Petit law [74.8 J/(K mol)].

Figure 1(b) shows the temperature dependence of C_p divided by the temperature, C_p/T, and entropy, S. Here, it was difficult to estimate a contribution from phonons and electrons other than $4f$ electrons using this data, because C_p/T is not proportional to T^2 at sufficiently low temperatures. The entropy released is 8.41 J/(K mol) at T_N, which is higher than $R\ln 2$ [5.76 J/(K mol)] but quite lower than $R\ln 4$ [11.5 J/(K mol)], where R is the gas constant. This result suggests that the phase transition at T_N is mainly caused by the spin degrees of freedom of the ground Kramers doublet.

Figure 2(a) shows the temperature dependence of magnetic susceptibility, χ, in a magnetic field of 0.1 T applied along [100] and [001]. Both χ follow the Curie-Weiss law at high temperatures. From Curie-Weiss fits, we obtained an effective magnetic moment, μ_{eff}, and a paramagnetic Curie temperature, θ_p (Table II).The obtained μ_{eff} is 10.8 and 10.7 μ_B in a field applied along [100] and [001], respectively. These values are almost the same value with the theoretical value of the free Dy^{3+}. Above T_N, χ in a field applied along [100] dominates χ along [001], indicating that the magnetically easy axis is [100]. χ along [100] exhibits a cusp-type anomaly at T_N. By contrast, χ along [001] displays an almost constant value below T_N, suggesting an AFM ordering in the (001) plane at T_N.

To investigate the AFM ordering at T_N, we measured χ at elevated magnetic fields applied along [100] and [001] [Figs. 2(b) and 2(c)]. T_N decreases monotonically as the field increases up to 2 T in a field applied along [100], confirming the AFM ordering. No cusp anomaly is detected down to 2 K at 3 T. In a field applied along [001], a kink at T_N is observed up until 3 T and T_N decreases with increasing fields [Fig. 2(c)].

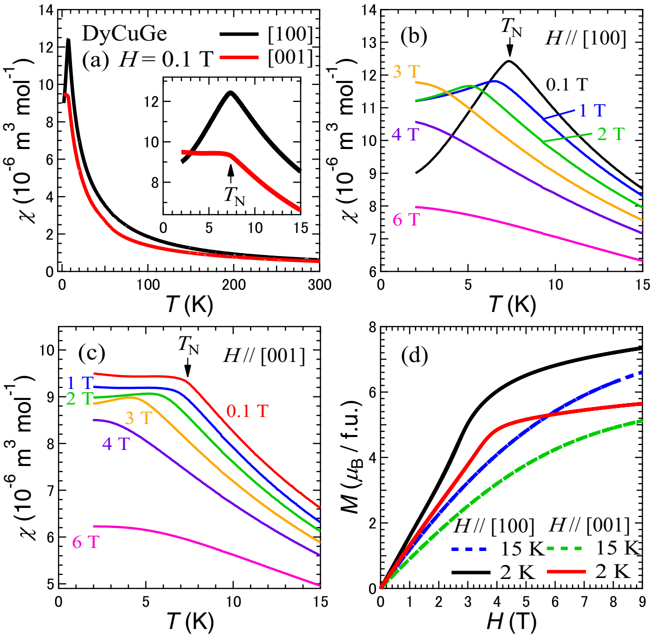

FIG. 2. Temperature dependence of the magnetic susceptibility measured (a) at 0.1 T below 300 K and at elevated magnetic fields applied along (b) [100] and (c) [001] below 15 K in DyCuGe. The inset represents the same data on an expanded temperature scale below 15 K. (d) Magnetization curves in fields applied along [100] and [001] up to 9 T at 2 and 15 K.

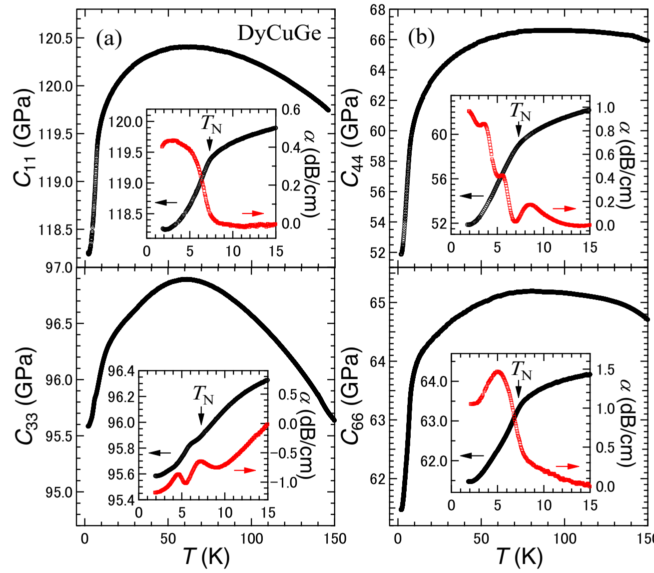

FIG. 3. Temperature dependence of (a) the longitudinal elastic moduli C_{11} and C_{33}, and (b) the transverse moduli C_{44} and C_{66} in DyCuGe. The insets represent the same data (left axis) on an expanded temperature scale below 15 K and its ultrasound attenuation α (right axis).

Here, χ along [001] at 0.1 and 1 T slightly increases below 4 K, whereas the data at 2 and 3 T decreases monotonically below T_N.

Figure 2(d) shows magnetization, M, curves at 2 and 15 K in fields applied along [100] and [001]. M curve at 2 K in a field applied along [100] displays a slight upturn around 2.6 T and reaches 7.3 μ_B at 9 T. This value is somewhat smaller than the saturated value of the Dy^{3+} (10.0 μ_B). In a field applied along [001], M curve at 2 K shows a kink below 4 T. The field derivative of the magnetization, dM/dH, exhibits a broad maximum around 2.6 and 3.3 T in fields applied along [100] and [001], respectively (not shown). At 15 K, both M curves increase monotonically with increasing fields. These results indicate that a critical magnetic field of the AFM phase boundary is between 2 and 3 T and between 3 and 4 T for fields applied along [100] and [001], respectively.

B. Elastic modulus and ultrasound attenuation

Figures 3(a) and 3(b) show the longitudinal and transverse elastic moduli, respectively, in DyCuGe. At high temperatures, all moduli increase monotonically as the temperature decreases. An elastic softening is detected below 60 and 80 K in the longitudinal and transverse moduli, respectively. The magnitude of the softening down to T_N is about 1% for the longitudinal moduli and 3% for C_{66}. In particular, the transverse modulus C_{44} exhibits a significant elastic softening with 11% reduction in the stiffness. The softening down to T_N is a characteristic behavior due to a quadrupole-mediated interaction in the CEF [7,9,12].

The insets of Figs. 3(a) and 3(b) show ultrasound attenuation, α, of each mode in the vicinity of T_N. The elastic modulus is also shown. C_{11}, C_{44}, and C_{66} change the slope at T_N, and then further soften down to 2 K. α of these modes increases below T_N and exhibits a peak around 4 K. In addition, α of C_{44} shows a bend around 6 K, just below T_N. Although the bend is reproducible suggesting an intrinsic behavior, its origin is unclear at present. Here, a broad peak is detected at below T_N in the specific heat [Fig. 1(a)]. The origin of the bend in α of C_{44} may cause some kind of contribution to the specific heat, resulting a possible broad peak. The longitudinal modulus C_{33} displays kinks around T_N, and its α has two peaks at T_N and around 4 K. A kink of C_{33} and a minimum of α around 6 K may be related to the bend in α of C_{44}.

It is noteworthy that a huge softening with 12% reduction is detected in C_{44} in contrast to other modes, which soften less than 3%. Such huge softening accompanied by ultrasound attenuation below T_N would be not attributed to a magnetic interaction, suggesting existence of a lattice instability in an AFM ordered state. Indeed, the C_{44} mode would be important to consider the ordered state in DyCuGe.

For further investigating the lattice instability below T_N, we measured the temperature dependence of C_{44} at elevated magnetic fields applied along [100] (Fig. 4). T_N, which is the temperature of the slope change in C_{44}, decreases by applying

TABLE II. Effective magnetic moment $\mu_{\rm eff}$ (μ_B) and paramagnetic Curie temperature θ_p (K) along [100] and [001] of DyCuGe obtained in the indicated temperatures range (K).

	$\mu_{\rm eff}$	θ_p	Temperature range
[100]	10.8	0.96	60–300
[001]	10.7	−30.5	100–300

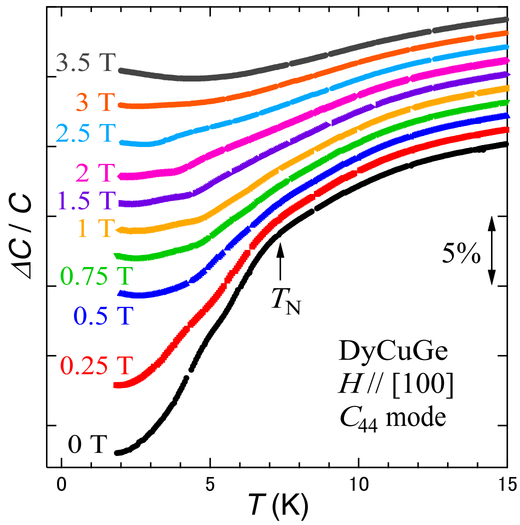

FIG. 4. Temperature dependences of the transverse modulus C_{44} at elevated magnetic fields applied along [100] in DyCuGe. We plotted C_{44} as relative change $\Delta C/C$. The data are shifted along the vertical axis for clarity.

fields, and then it becomes unclear around 1 T. Beyond T_N the magnitude of the softening is hardly changed. By contrast, the softening below T_N is drastically suppressed at elevated magnetic fields. α of C_{44} is also reduced as the field increases (not shown). These results manifest that the lattice instability in the AFM ordered state is lifted by the magnetic field.

C. Crystal-electric-field effects

To clarify the origin of the lattice instability in the AFM ordered state, we first conducted the CEF fits using the data of the transverse moduli, $1/\chi$, and M curves above T_N, i.e., in the nonordered state. We adopted the hexagonal CEF of the C_{6v} point symmetry to simplify the analysis. We consider the following effective Hamiltonian:

$$H_{\mathrm{eff}} = H_{\mathrm{CEF}} + H_{\mathrm{Q}} + H_{\mathrm{Zeeman}}$$
$$H_{\mathrm{CEF}} = B_2^0 O_2^0 + B_4^0 O_4^0 + B_6^0 O_6^0 + B_6^6 O_6^6$$
$$H_{\mathrm{Q}} = -\sum_i g_i O_i \varepsilon_i - \sum_i g_i' \langle O_i \rangle O_i \;\; (i = 4, 6)$$
$$H_{\mathrm{Zeeman}} = -g_J \mu_B J \cdot H,$$

where H_{CEF}, H_{Q}, and H_{Zeeman} are Hamiltonians of the CEF, the quadrupole-mediated interaction, and the Zeeman interaction, respectively. Here, ε_i is the strain, g_i is the strain-quadrupole coupling constant, g_i' is the quadrupole-quadrupole coupling constant, O_i is the electric-quadrupole operator, B_m^n is the CEF parameter, and O_m^n is the Stevens equivalent operators, respectively [33]. $\langle O_i \rangle$ represents a thermal average of the operator. The subscripts $i = 4$ and 6 are equal to yz and xy, respectively. C_{44} and C_{66} are the linear responses to the ε_{yz} (ε_{zx}) and ε_{xy} ($\varepsilon_{xx} - \varepsilon_{yy}$) strains, which couple to the electric quadrupoles O_{yz} (O_{zx}) and O_{xy} (O_2^2), respectively, in the hexagonal symmetry. The quadrupole-mediated interaction term H_{Q} is used only for the elastic moduli. The temperature dependence of the elastic modulus, C_{ii}, in the nonordered state was calculated

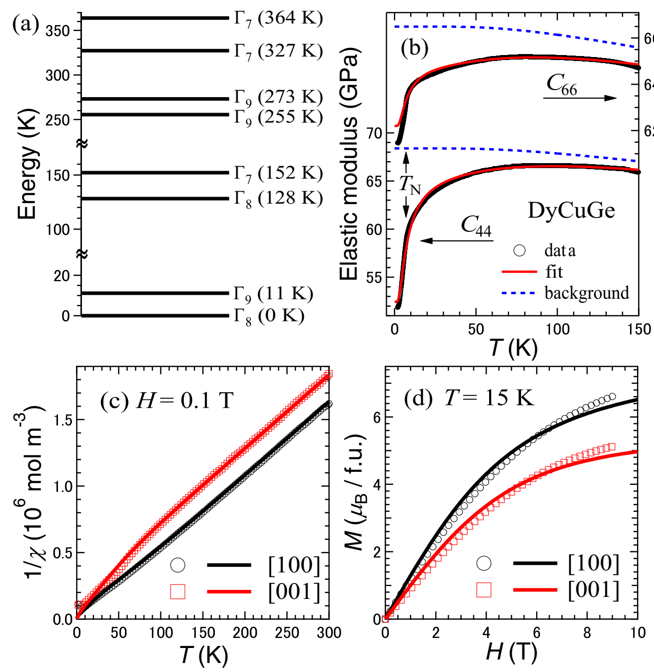

FIG. 5. (a) $4f$ level scheme for DyCuGe obtained from the CEF parameters listed in Table III, where Γ_i denotes the irreducible representation for the point symmetry C_{6v}. (b) Temperature dependence of the transverse elastic moduli. The red solid and blue dashed lines represent the fit result and the background stiffness, respectively. (c) Temperature dependence of the inverse magnetic susceptibility measured at 0.1 T. (d) Magnetization curves at 15 K. Solid lines demonstrate the calculated results.

using the following equation:

$$C_{ii}(T) = C_0 \left[\frac{1 - \left(N_0 g_i^2 / C_0 + g_i' \right) \chi_s(T)}{1 - g_i' \chi_s(T)} \right]$$
$$C_0(T) = C_{0\mathrm{K}} - \frac{s}{\exp(\theta_D / T) - 1},$$

where N_0 ($= 1.77 \times 10^{28}$ m^{-3}) is the number of Dy^{3+} per unit volume and χ_s is the so-called strain susceptibility [34,35]. For the background stiffness, $C_0(T)$, we used the Varshni equation, where $C_{0\mathrm{K}}$ is the elastic modulus at 0 K, θ_D is the Debye temperature, and s is a fit parameter [36,37].

We repeated the CEF fits using different initial CEF parameter values to reproduce the data. The obtained CEF-level scheme is the ground doublet Γ_8, the first excited doublet Γ_9 at 11 K, the second excited doublet Γ_8 at 128 K, and many others [Fig. 5(a)]. The red solid curves in Fig. 5(b) are the best fits for C_{44} and C_{66} in the nonordered state. The calculated results well reproduce the data above T_N by the fit parameters listed in Tables III and IV. Here, we adopted the value of $\theta_D = 244$ K obtained from the sound velocity (Table I). It is noted

TABLE III. CEF parameters of DyCuGe in Kelvin.

B_2^0	B_4^0	B_6^0	B_6^6
0.44	7.50×10^{-3}	-1.00×10^{-4}	-3.20×10^{-4}

TABLE IV. Fit parameters for the transverse moduli: $|g_i|$ (K), g_i' (K), C_{0K} (GPa), and s (GPa).

	$\|g_i\|$	g_i'	C_{0K}	s
C_{44} (O_{yz}, O_{zx})	41.6	5.00 $\times 10^{-3}$	68.4	5.50
C_{66} (O_{xy}, O_2^2)	41.8	2.00 $\times 10^{-2}$	66.5	3.73

that the only ground Kramers doublet does not produce elastic softening because it has no quadruple degeneracy. Our fit results reveal that interlevel quadrupole-mediated interactions between the ground and excited doublets cause the softening of both moduli above T_N, and corresponding quadrupoles affect physical properties in DyCuGe. The interactions of these quadrupoles are of ferroquadrupolar-type because of the positive sign of g' (Table IV).

On the other hand, the longitudinal moduli C_{11} and C_{33} also show the softening from 60 K to T_N. C_{11} and C_{33} are mixed modes of [$(C_{11}$-$C_{12})/2$, C_B, C_u] and [C_B, C_u], respectively, where C_B and C_u are responses to the $\varepsilon_B = \varepsilon_{xx} + \varepsilon_{yy} + \varepsilon_{zz}$ and $\varepsilon_u = (3\varepsilon_{zz} - \varepsilon_B)/\sqrt{3}$ strains, respectively [38]. Here, C_{66} and $(C_{11}$-$C_{12})/2$ are degenerate in the hexagonal symmetry. $(C_{11}$-$C_{12})/2$ and C_u are elastic modes corresponding to the electric quadrupoles O_2^2 and O_2^0, respectively. The softening of the longitudinal moduli above T_N would be due to quadrupole-mediated interactions of O_2^2 and O_2^0, or a softening of the bulk modulus, C_B.

We calculated $1/\chi$ and M using the aforementioned CEF model: $H_{CEF} + H_{Zeeman}$ [39,40]. Figures 5(c) and 5(d) illustrate the fit results for $1/\chi$ in 0.1 T and M curves at 15 K, respectively. The experimental $1/\chi$ data and theoretical calculations are consistent above T_N in both $1/\chi$ [Fig. 5(c)]. The M data at 15 K are almost reproduced including magnetic anisotropy [Fig. 5(d)]. From these results, we revealed the $4f$ electronic state in DyCuGe reproducing the transverse moduli, $1/\chi$, and M curves in the nonordered state.

The first excited doublet exists at 11 K, which is relatively higher than the energy scale of T_N [Fig. 5(a)]. The ground Kramers doublet Γ_8 possesses spin interactions of J_x and J_y at zero field, where J_l is an angular-momentum operator and subscripts $l = x$, y, and z correspond to [100], [120], and [001], respectively. At T_N an AFM ordering in the (001) plane has been proposed (Sec. III A). The phase transition at T_N is caused by the spin degrees of freedom of the ground Kramers doublet Γ_8.

D. Lattice instability in an antiferromagnetically ordered state

Further, we discuss the origin of the lattice instability in the AFM ordered state. In our experimental results, C_{44} shows a huge softening accompanied by ultrasound attenuation below T_N, which is lifted by the magnetic field. To examine an influence of the electric quadrupoles O_{yz} and O_{zx} corresponding to C_{44} for the lattice instability, we calculated the specific heat, entropy, and spontaneous expectation values of J_x, J_y, J_z, O_{yz}, and O_{zx} using the equation consisting of $H_{CEF} + H_{ex}$. Here, H_{ex} is the Hamiltonian of the spin and quadrupole exchange

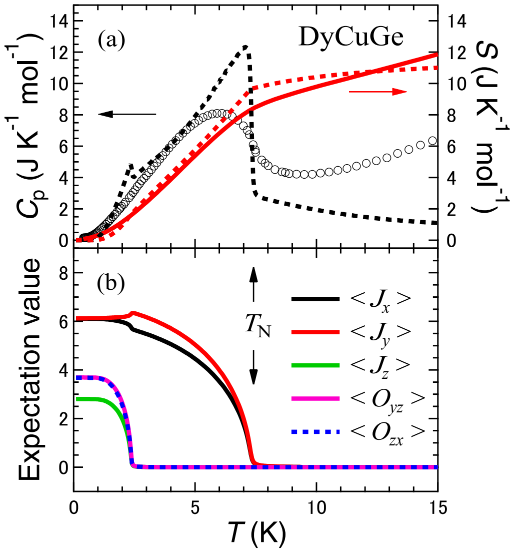

FIG. 6. (a) Temperature dependence of C_p (left axis) and entropy (right axis). Open circles and solid line are the same data with Fig. 1. The dashed lines demonstrate the calculated results of $4f$ contribution. (b) Temperature dependence of spontaneous expectation values of J_x, J_y, J_z, O_{yz}, and O_{zx} at zero magnetic field within our calculations.

interactions in the mean-field approximation:

$$H_{ex} = -\sum_{j=A,B}\Big[J_{exx}^{AB}\langle J_x\rangle^{(j)}J_x + J_{exy}^{AB}\langle J_y\rangle^{(j)}J_y + J_{exz}^{AB}\langle J_z\rangle^{(j)}J_z + \sum_i g_{ex}^{AB}\langle O_i\rangle^{(j)}O_i\Big],$$

where J_{exl}^{AB} and g_{ex}^{AB} are the coupling constants of intersublattice spin and quadrupole exchange interactions, respectively. The symbols A and B denote two sublattices [41].

Figure 6(a) shows the calculated specific heat and entropy of $4f$ contribution at zero magnetic field. The transition temperature of T_N and entropy are qualitatively reproduced using $J_{exx}^{AB} = J_{exy}^{AB} = -0.5$ K, $J_{exz}^{AB} = -0.3$ K, $g_{ex}^{AB} = 5.00 \times 10^{-3}$ K, and the obtained CEF parameters (Table III). Here, negative values for J_x and J_y reflect the proposed magnetic structure, which is the AFM ordering in the (001) plane. The negative θ_p value along [001] is considered for J_z (Table II), which is assumed to be smaller than the values of J_x and J_y. We used the obtained g' for g_{ex}^{AB} of both electric quadrupoles O_{yz} and O_{zx} (Table IV).

As the temperature decreases, spontaneous expectation values of J_x and J_y occur at T_N [Fig. 6(b)], being in line with the AFM ordering in the (001) plane. Within our calculations, spontaneous expectation values of J_z, O_{yz}, and O_{zx} simultaneously emerge far below T_N. Actually, quadrupolar ordering may not occur in DyCuGe, because C_p displays no clear anomaly below T_N (Fig. 1). However, it is noteworthy that ferroquadrupolar interactions of O_{yz} and O_{zx}, of which a phase transition can occur, survive below T_N.

In almost all compounds, quadrupole-mediated interactions are lifted by a magnetic ordering because the CEF states are split by a local internal magnetic field, resulting disappearance of the softening. By contrast, we recently discovered that the heavy-rare-earth compound ErNiAl displays a large softening in a magnetically ordered state and undergoes a ferroquadrupolar ordering [13]. This is because the wave functions of the CEF states are mixed by an energy of the emerged internal field. ErNiAl contains a strong quadrupole-mediated interaction showing a substantial softening. As a result, separated two states of the ground Kramers doublet have the quadrupole-mediated interaction below the magnetic transition temperature, then an elastic softening appears.

DyCuGe also possesses strong quadrupole-mediated interactions of O_{yz} and O_{zx}, giving rise to the significant softening with 11% reduction above T_N [Fig. 3(b)]. Since the first excited doublet exists at 11 K, quadrupole-mediated interactions of O_{yz} and O_{zx} would occur between the ground two states split by an internal magnetic field of the magnetic ordering. g' for O_{yz} and O_{zx} is positive (Table IV). Thereby, the huge softening of C_{44} below T_N would arise from a ferroquadrupolar lattice instability.

By applying magnetic fields, quadrupole-mediated interactions are often weakened by further splitting of the ground two states by the Zeeman energy. In fact, the ferroquadrupolar lattice instability in DyCuGe is lifted by the magnetic field (Fig. 4). On the other hand, the ferroquadrupolar lattice instability may result in a slight increase below 4 K in χ at 0.1 and 1 T along [001] [Fig. 2(c)]. χ at 2 and 3 T decreases below T_N due to disappearance of the instability by the magnetic field.

In DyCuGe, the magnitude of an energy splitting of the ground Kramers doublet due to the magnetic ordering is calculated to be 8 K within our CEF model with the mean-field approximation. This value corresponds to an energy splitting by an external magnetic field of 3 T in the (001) plane. Because the internal magnetic field emerged is small and quadrupole-mediated interactions are strong, a quadrupolar instability occurs in a magnetically ordered state. This scenario would be applied to rare-earth compounds in a similar situation, and those have a possibility of multipolar ordering even in a magnetically ordered state, such as ErNiAl.

Consequently, we succeeded to synthesize a single-crystalline DyCuGe with an antiferromagnetic ordering in the (001) plane at 7.4 K. We reveal a O_{yz} (O_{zx})-type ferroquadrupolar lattice instability in the antiferromagnetically ordered state in DyCuGe.

IV. CONCLUSION

We synthesized a single-crystalline DyCuGe with localized $4f$ electrons. We measured the specific heat and magnetic properties of DyCuGe and determined an antiferromagnetic ordering in the (001) plane at T_N. A prominent elastic softening above T_N was found in all moduli. From the theoretical analysis using the CEF model, we clarified the $4f$ electronic state in DyCuGe, indicating that the softening is due to interlevel quadrupole-mediated interactions between the CEF states. Furthermore, a huge softening accompanied by ultrasound attenuation was detected below T_N in C_{44}, suggesting a lattice instability. The huge softening is not caused by a magnetic interaction, however, it is lifted by the magnetic field. The plausible scenario is that a O_{yz} (O_{zx})-type ferroquadrupolar lattice instability appears due to quadrupole-mediated interactions between the ground two states separated by an internal magnetic field of the magnetic ordering.

ACKNOWLEDGMENTS

This work was supported by JSPS KAKENHI Grant No. 22K03485. The work was supported by MGML [42] within the Program of Czech Research Infrastructures (Project No. LM2018096). The authors acknowledge the assistance provided by the Ferroic Multifunctionalities Project No. CZ.02.01.01/00/22_008/0004591.

[1] H. Sato, H. Sugawara, Y. Aoki, and H. Harima, in *Handbook of Magnetic Materials*, edited by K. H. J. Buschow (North Holland, Amsterdam, 2009), Vol. 18, Chap. 1.
[2] Y. Kuramoto, H. Kusunose, and A. Kiss, Multipole orders and fluctuations in strongly correlated electron systems, J. Phys. Soc. Jpn. **78**, 072001 (2009).
[3] T. Onimaru and H. Kusunose, Exotic quadrupolar phenomena in non-Kramers doublet systems –the cases of PrT_2Zn_{20} (T = Ir, Rh) and PrT_2Al_{20} (T = V, Ti)–, J. Phys. Soc. Jpn. **85**, 082002 (2016).
[4] S. Hayami, M. Yatsushiro, Y. Yanagi, and H. Kusunose, Classification of atomic-scale multipoles under crystallographic point groups and application to linear response tensors, Phys. Rev. B **98**, 165110 (2018).
[5] S. Hayami and H. Kusunose, Microscopic description of electric and magnetic toroidal multipoles in hybrid orbitals, J. Phys. Soc. Jpn. **87**, 033709 (2018).
[6] M. T. Suzuki, T. Nomoto, R. Arita, Y. Yanagi, S. Hayami, and H. Kusunose, Multipole expansion for magnetic structures: A generation scheme for a symmetry-adapted orthonormal basis set in the crystallographic point group, Phys. Rev. B **99**, 174407 (2019).
[7] I. Ishii, K. Takezawa, T. Mizuno, S. Kamikawa, H. Ninomiya, Y. Matsumoto, S. Ohara, K. Mitsumoto, and T. Suzuki, Ferroquadrupolar ordering due to the quasi-degenerate quartet in the trigonal chiral structure of $DyNi_3Ga_9$, J. Phys. Soc. Jpn. **87**, 013602 (2018).
[8] I. Ishii, K. Takezawa, T. Mizuno, S. Kumano, T. Suzuki, H. Ninomiya, K. Mitsumoto, K. Umeo, S. Nakamura, and S. Ohara, Anisotropic phase diagram of ferroquadrupolar ordering in the trigonal chiral compound $DyNi_3Ga_9$, Phys. Rev. B **99**, 075156 (2019).
[9] I. Ishii, T. Mizuno, K. Takezawa, S. Kumano, Y. Kawamoto, T. Suzuki, D. I. Gorbunov, M. S. Henriques, and A. V. Andreev, Magnetic-field-induced quadrupolar ordering and the crystal electric field effect in the distorted kagome lattice antiferromagnet $Dy_3Ru_4Al_{12}$, Phys. Rev. B **97**, 235130 (2018).
[10] I. Ishii, T. Suzuki, A. V. Andreev, D. I. Gorbunov, K. Mitsumoto, K. Araki, A. Miyata, D. I. Gorbunov, S. Zherlitsyn, and J. Wosnitza, Magnetic field induced reentrant

multipolar ordering in the distorted kagome-lattice antiferromagnet $Dy_3Ru_4Al_{12}$, Phys. Rev. B **107**, 205136 (2023).
[11] D. I. Gorbunov, I. Ishii, Y. Kurata, A. V. Andreev, T. Suzuki, S. Zherlitsyn, and J. Wosnitza, Crystal-field effects in $Er_3Ru_4Al_{12}$ with a distorted kagome lattice, Phys. Rev. B **101**, 094415 (2020).
[12] I. Ishii, D. Suzuki, T. Umeno, Y. Kurata, Y. Wada, T. Suzuki, A. V. Andreev, D. I. Gorbunov, A. Miyata, S. Zherlitsyn, and J. Wosnitza, Distinct field-induced ferroquadrupolar states for two different magnetic-field directions in DyNiAl, Phys. Rev. B **103**, 195151 (2021).
[13] I. Ishii, Y. Kurata, Y. Wada, M. Nohara, T. Suzuki, K. Araki, and A. V. Andreev, Ferroquadrupolar ordering in a magnetically ordered state in ErNiAl, Phys. Rev. B **105**, 165147 (2022).
[14] D. I. Gorbunov, S. Palazzese, I. Ishii, A. V. Andreev, J. Šebek, V. Buturlim, T. Suzuki, S. Zherlitsyn, and J. Wosnitza, Magnetic and magnetoelastic properties of Er_3Al_2, Phys. Rev. Mater. **6**, 084409 (2022).
[15] M. Tsukagoshi, T. Matsumura, S. Michimura, T. Inami, and S. Ohara, Competition between helimagnetic and ferroquadrupolar ordering in a monoaxial chiral magnet $DyNi_3Ga_9$ studied by resonant x-ray diffraction, Phys. Rev. B **105**, 014428 (2022).
[16] A. Iandelli, The structure of ternary phases of rare earths with RCuGe composition, J. Alloys Compd. **198**, 141 (1993).
[17] A. V. Lukoyanov, L. N. Gramateeva, Y. V. Knyazev, Y. I. Kuzmin, S. Gupta, and K. G. Suresh, Effect of electronic correlations on the electronic structure, magnetic and optical properties of the ternary *R*CuGe compounds with R = Tb, Dy, Ho, Er, Materials **13**, 3536 (2020).
[18] S. Baran, A. Szytula, J. Leciejewicz, N. Stüsser, A. Zygmunt, Z. Tomkowicz, and M. Guillot, Magnetic structures of *R*CuGe (R = Pr, Nd, Tb, Dy, Ho and Er) compounds from neutron diffraction and magnetic measurements, J. Alloys Compd. **243**, 112 (1996).
[19] S. Baran, A. Szytula, J. Leciejewicz, N. Stüsser, A. Zygmunt, Z. Tomkowicz, and M. Guillot, Magnetic structures of RCuGe (R = rare earth) compounds, Phys. B: Condens. Matter **234-236**, 656 (1997).
[20] S. Gupta and K. G. Suresh, Variations of magnetocaloric effect and magnetoresistance across *R*CuGe (R = Tb, Dy, Ho, Er) compounds, J. Magn. Magn. Mater. **391**, 151 (2015).
[21] Y. Nemoto, T. Yamaguchi, T. Horino, M. Akatsu, T. Yanagisawa, T. Goto, O. Suzuki, A. Dönni, and T. Komatsubara, Ferroquadrupole ordering and Γ_5 rattling motion in the clathrate compound $Ce_3Pd_{20}Ge_6$, Phys. Rev. B **68**, 184109 (2003).
[22] Y. Nakanishi, T. Sakon, M. Motokawa, M. Ozawa, T. Suzuki, and M. Yoshizawa, Elastic properties and phase diagram of the rare-earth monopnictide TbSb, Phys. Rev. B **68**, 144427 (2003).
[23] T. Yanagisawa, T. Goto, Y. Nemoto, S. Miyata, R. Watanuki, and K. Suzuki, Ultrasonic investigation of quadrupole ordering in HoB_2C_2, Phys. Rev. B **67**, 115129 (2003).
[24] T. Goto, Y. Nemoto, K. Sakai, T. Yamaguchi, M. Akatsu, T. Yanagisawa, H. Hazama, K. Onuki, H. Sugawara, and H. Sato, Quadrupolar effect and rattling motion in the heavy-fermion superconductor $PrOs_4Sb_{12}$, Phys. Rev. B **69**, 180511(R) (2004).
[25] M. Akatsu, T. Goto, O. Suzuki, Y. Nemoto, S. Nakamura, S. Kunii, and G. Kido, Magnetic anisotropy of the antiferroquadrupole phase in $Ce_{0.50}La_{0.50}B_6$, Phys. Rev. Lett. **93**, 156409 (2004).
[26] I. Ishii, H. Muneshige, Y. Suetomi, T. K. Fujita, T. Onimaru, K. T. Matsumoto, T. Takabatake, K. Araki, M. Akatsu, Y. Nemoto, T. Goto, and T. Suzuki, Antiferro-quadrupolar ordering at the lowest temperature and anisotropic magnetic field-temperature phase diagram in the cage compound $PrIr_2Zn_{20}$, J. Phys. Soc. Jpn. **80**, 093601 (2011).
[27] I. Ishii, H. Muneshige, S. Kamikawa, T. K. Fujita, T. Onimaru, N. Nagasawa, T. Takabatake, T. Suzuki, G. Ano, M. Akatsu, Y. Nemoto, and T. Goto, Antiferroquadrupolar ordering and magnetic-field-induced phase transition in the cage compound $PrRh_2Zn_{20}$, Phys. Rev. B **87**, 205106 (2013).
[28] S. Kamikawa, I. Ishii, K. Takezawa, T. Mizuno, T. Sakami, F. Nakagawa, H. Tanida, M. Sera, T. Suzuki, K. Mitsumoto, and X. Xi, Elastic softening due to the quadrupole interaction and anomalous magnetic phase diagram under the magnetic field in $HoRu_2Al_{10}$, Phys. Rev. B **96**, 155131 (2017).
[29] D. I. Gorbunov, I. Ishii, T. Nomura, M. S. Henriques, A. V. Andreev, M. Uhlarz, T. Suzuki, S. Zherlitsyn, and J. Wosnitza, Magnetic phase diagram and crystal-field effects in the kagome-lattice antiferromagnet $U_3Ru_4Al_{12}$, Phys. Rev. B **99**, 054413 (2019).
[30] T. J. Moran and B. Lüthi, Elastic and magnetoelastic effects in magnetite, Phys. Rev. **187**, 710 (1969).
[31] B. Wolf, B. Lüthi, S. Schmidt, H. Schwenk, M. Sieling, S. Zherlitsyn, and I. Kouroudis, New experimental techniques for pulsed magnetic fields – ESR and ultrasonics, Phys. B: Condens. Matter **294-295**, 612 (2001).
[32] B. Lüthi, in *Physical Acoustics in the Solid State* (Springer, Heidelberg, 2005), Chap. 4.
[33] M. T. Hutchings, Point-charge calculations of energy levels of magnetic ions in crystalline electric fields, Solid State Phys. **16**, 227 (1964).
[34] B. Lüthi, in *Dynamical Properties of Solids*, edited by G. K. Horton and A. A. Maradudin (North-Holland, Amsterdam, 1980), Chap. 4.
[35] See Supplemental Material of Ref. [8].
[36] Y. P. Varshni, Temperature dependence of the elastic constants, Phys. Rev. B **2**, 3952 (1970).
[37] Z. Zhang, V. Keppens, and T. Egami, A simple model to predict the temperature dependence of elastic moduli of bulk metallic glasses, J. Appl. Phys. **102**, 123508 (2007).
[38] T. Suzuki, I. Ishii, N. Okuda, K. Katoh, T. Takabatake, T. Fujita, and A. Tamaki, Quadrupolar ordering of $5f$ electrons in UCu_2Sn, Phys. Rev. B **62**, 49 (2000).
[39] N. V. Hieu, T. Takeuchi, H. Shishido, C. Tonohiro, T. Yamada, H. Nakashima, K. Sugiyama, R. Settai, T. D. Matsuda, Y. Haga, M. Hagiwara, K. Kindo, S. Araki, Y. Nozue, and Y. Ōnuki, Magnetic properties and crystalline electric field scheme in $RRhIn_5$ (R: Rare Earth), J. Phys. Soc. Jpn. **76**, 064702 (2007).
[40] S. Kamikawa, I. Ishii, Y. Noguchi, H. Goto, T. K. Fujita, F. Nakagawa, H. Tanida, M. Sera, and T. Suzuki, Elastic softening in $HoFe_2Al_{10}$ due to the quadrupole interaction under an orthorhombic crystal electric field, J. Phys. Soc. Jpn. **85**, 074604 (2016).
[41] M. Sera, H. Nohara, M. Nakamura, H. Tanida, T. Nishioka, and M. Matsumura, Unusual temperature-dependent exchange interaction in $GdFe_2Al_{10}$ in comparison with $GdRu_2Al_{10}$, Phys. Rev. B **88**, 100404(R) (2013).
[42] See https://mgml.eu.